



# Holocene fire regimes across the Altai-Sayan Mountains and adjacent plains: interaction with climate and vegetation types

Dongliang Zhang<sup>1,2,3</sup>, Blyakharchuk Tatiana<sup>4</sup>, Aizhi Sun<sup>5</sup>, Xiaozhong Huang<sup>6</sup>, and Yuejing Li<sup>1,2,3</sup>

<sup>1</sup>State Key Laboratory of Ecological Safety and Sustainable Development in Arid Lands, Xinjiang Institute of Ecology and Geography, Chinese Academy of Sciences, 818 Beijing South Road, Urumqi, China

<sup>2</sup>Research Center for Ecology and Environment of Central Asia, Chinese Academy of Sciences, 818 Beijing South Road, Urumqi, China

<sup>3</sup>University of Chinese Academy of Sciences, 19A Yuquan Road, Beijing, China

<sup>4</sup>Institute of Monitoring of Climatic and Ecological Systems, Siberian Branch of Russian Academy of Sciences, Tomsk, Russia

<sup>5</sup>College of Earth and Planetary Sciences, University of Chinese Academy of Sciences, Beijing, China

<sup>6</sup>College of Earth and Environmental Sciences, Lanzhou University, Lanzhou, China

**Correspondence:** Dongliang Zhang (zhdl@ms.xjb.ac.cn) and Aizhi Sun (aizhisun@ucas.ac.cn)

Received: 28 April 2025 – Discussion started: 26 May 2025

Revised: 2 February 2026 – Accepted: 9 February 2026 – Published: 4 March 2026

**Abstract.** The Altai-Sayan Mountains and adjacent plains (including the west Siberian Plain, Kazakhstan Hills and Junggar Basin) have experienced accelerated warming in recent decades, raising growing concerns about escalating wildfire risks. However, two key gaps hinder understanding: paleofire dynamics in western Mongolia are understudied and no comprehensive regional synthesis exists for charcoal influx across the Altai-Sayan ecoregion. To address this, we reconstructed the Holocene fire sequence in western Mongolia and analyzed the spatiotemporal variations in charcoal influx across different vegetation zones of the Altai-Sayan Mountains and adjacent plains, as well as their coupling relationships with vegetation structure. The results reveal that Holocene declines in charcoal influx were driven by distinct mechanisms across subregions: above the forest limit in the central Altai Mountains, the decline was primarily controlled by temperature-limited woody biomass availability; in the western Sayan Mountains, it stemmed from the substantial expansion of fire-resistant *P. sylvestris*. Since  $\sim 2$  cal. kyr BP, intensified anthropogenic disturbances – specifically agricultural expansion and pastoral activities – have significantly increased fire frequency in the southeastern, western and northern Altai Mountains, the west Siberian Plain and the forest zones of central Altai Mountains. Conversely, the marked decline in charcoal influx observed in the

Khangai Mountains may be closely associated with vegetation fragmentation caused by overgrazing. Our findings provide a long-term perspective on fire-vegetation-climate interactions, offering critical insights for sustainable land management in the Altai-Sayan ecoregion.

## 1 Introduction

The North Europe-Siberia-Altai region is the core distribution area of boreal forest ecosystems, hosting over 90 % of the continent's boreal forest biomass and terrestrial organic carbon stocks (Furyaev, 1996; Kasischke, 2000). Its dynamics are closely intertwined with global climate system, forming a critical positive feedback loop. In 2021, wildfires in the global boreal forests released 1.76 PgCO<sub>2</sub>, setting a historical record at that time (Zheng et al., 2023). Notably, the majority of carbon emissions from boreal forests originated from northern Eurasia. Carbon sequestration gain from a prolonged growing season may not offset carbon loss caused by enhanced respiration and disturbances (Mo et al., 2023). This ecological transformation triggers critical climate feedback mechanisms through carbon pool transformation, cascading ecological and permafrost degradation (Ivanova et al., 2020; Jones et al., 2020). This shift not only threatens regional car-

bon balance but also significantly accelerates global warming by releasing massive amounts of greenhouse gases, underscoring the extreme urgency of protecting this ecosystem for stabilizing the global climate.

Within this crucial northern Eurasian context, the Altai-Sayan region lies at the junction of Arid Central Asia and the boreal forest ecosystems. This region features an extremely steep hydrothermal gradient ranging from warm, arid steppes/shrublands in the south to cold, humid closed-canopy boreal forests in the north, forming a vast and sensitive ecotone (Xinjiang Comprehensive Expedition Team, Institute of Botany, Chinese Academy of Sciences, 1978). It is precisely this “marginal” and “transitional” nature that makes it a natural laboratory and early warning system for studying fire-climate interactions (Fu et al., 2013; Liu et al., 2021). The convergence of two key flammability drivers—coniferous vegetation (*Pinus sibirica* dominance > 60%) and intensifying drought regimes has created a pyrogeographic hotspot. This synergy amplifies fire return intervals by  $2.3\times$  compared to pre-1990 baselines, fundamentally altering successional pathways and threatening ecological security thresholds (Goldammer and Furyaev, 2013).

Remote sensing analyses document a quadrupling of fire events from  $712 \pm 89 \text{ yr}^{-1}$  (1980–2000) to  $3024 \pm 214 \text{ yr}^{-1}$  (2001–2020) with burned area expanding exponentially ( $R^2 = 0.91$ ,  $p < 0.001$ ) (Ponomarev and Kharuk, 2016), which has a phase coincidence with the dynamics of mean temperatures and climate dryness (Ponomarev and Kharuk, 2016). In the southern Altai, the reduced burned area since 1987 can be attributed to increased moisture and greatly increased investment in fire prevention (Shi et al., 2020). The dynamic changes of fires in the instrumental measurement period driven by human activities and natural processes exhibit distinct differences. However, contemporary observations remain circumscribed by the temporal resolution limitations of satellite archives (post-1980) and instrumental records, creating a < 50-year observational window that inadequately captures decadal-scale fire-climate-human feedbacks (Shi et al., 2020; Ponomarev and Kharuk, 2016; Albrich et al., 2018; Kharuk et al., 2021). These both limit our understanding of long-term fire activities in the ecological sensitivity regions.

Paleoecological approaches spanning centennial to millennial timescales provide crucial temporal dimensional support for disentangling the complex interactions through pattern-process analysis. Existing Holocene fire records in the Altai-Sayan ecoregion have established a robust methodological framework for reconstructing fire-vegetation-climate couplings (e.g., Blyakharchuk et al., 2004, 2007, 2008; Hu et al., 2025; Li et al., 2024). However, two critical knowledge gaps remain to be addressed: (1) the complete fire sequence in western Mongolia, and (2) the spatiotemporal linkages between fire in this region and montane ecosystem dynamics across the Altai-Sayan ecoregion. To address this issue, this study selected Achit Nuur as the study site

because of its continuous and stable depositional environment. Three critical research dimensions include in this study: (1) Reconstructing fire variability in the Holocene interval ( $\sim 11.75\text{--}0 \text{ cal. kyr BP}$ ) using high-resolution microscopic charcoal analysis from Achit Nuur; (2) Identifying ecotonal heterogeneity in fire regimes through comparison with other already-published paleofire records ( $n = 23$ ) in the nearby regions; (3) Evaluating how dominant tree genera (*Abies*, *Betula*, *Larix*, *Picea*, *P. sibirica*, *P. sylvestris*) and their summed percentages as forest cover modulate fire characteristics across vegetation types. This study will clarify the long-timescale fire history in the Altai-Sayan ecoregion, as well as its complex associations with climate fluctuations, vegetation succession and human activities. These outputs provide empirical foundations for developing climate-responsive fire management strategies in the Central Asian ecosystems under the future scenarios.

## 2 Physiographic Settings

### 2.1 The Altai-Sayan Mountains

The Altai-Sayan Mountains, one of the most prominent mountain ranges in Central Asia, connect with the Kazakhstan Hills to the west, border the Southern Siberian Plain to the north, and adjoin the Junggar Basin-Khangai Mountains to the south (Fig. 1; Feng et al., 2017). Climatologically, this region holds great significance, as it likely served as a transitional zone where the Westerlies-dominated climates from the west interacted with the Asian Monsoon-influenced climates from the east during the Holocene (Blyakharchuk et al., 2004, 2008; Zhang and Zhang, 2025). Culturally, it also functioned as a cultural crossroads between Asian and European civilizations along the “Eurasian Steppe Silk Road” (Blyakharchuk and Chernova, 2013; Xiang et al., 2023).

The North Atlantic Oscillation and Siberian High drive the southward displacement of the Westerlies, which transport water vapor from the Mediterranean, Caspian, and Black Seas into the study region during winter and spring (Aizen et al., 2001; Kutzbach et al., 2014). In contrast, the interaction between the Asian Low and Azores High regulates the northward shift of the Westerlies, facilitating water vapor transport in summer and autumn (Aizen et al., 2001). These latitudinal shifts of the westerlies induce a southward gradient of decreasing precipitation and increasing climatic aridity, which in turn shapes the characteristic vegetation distribution patterns across the Central Asia (Fig. 1). Zonally, vegetation distribution exhibits a strong latitudinal dependence. Specifically, the coniferous forests dominate the southern Siberian Plain, while the eastern Kazakhstan Hills and western Mongolia are characterized by steppe ecosystems, and the Junggar Basin is covered by desert-steppe (Chen, 2010). Additionally, the region’s vegetation displays distinct vertical zonation with communities transitioning from desert and steppe at lower elevations to forest and alpine meadow at

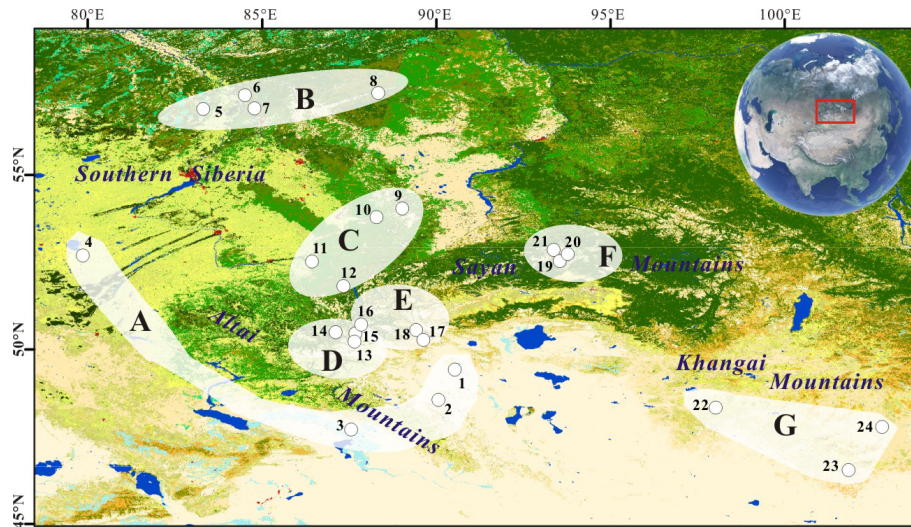


**Figure 1.** Spatial distributions of the selected fossil pollen/charcoal sequences across the Altai-Sayan Mountains and adjacent plains. Region A: Achit Nuur (1), Tolbo Lake (2), Alahake Lake (3) and Kuchuk Lake (4); Region B: Rybnaya Mire (5), Plotnikovo Mire (6), Shchuchye Lake (7) and Ulukh–Chayakh Mire (8); Region C: Chudnoye Mire (9), Tundra Mire (10), Mokhovoe Bog (11) and Kuantang Mire (12); Region D: Dzhangyskol Lake (13), Uzunkol Lake (14) and Kendegelukol Lake (15); Region E: Tashkol Lake (16), Akkol Lake (17) and Grusha Lake (18); Region F: Buibinskoye Mire (19), Bezrybnoye Mire (20) and Lugovoe Peat (21); Region G: Olgi Lake (OL3) (22), Shireet Naiman Nuur (23) and Uggi Nuur (24).

higher elevations (Blyakharchuk and Chernova, 2013; Zhang et al., 2020).

## 2.2 Achit Nuur

Achit Nuur (49.42° N, 90.52° E; 1444 m a.s.l.) occupies an intermountain basin bounded by the Mongolian Altai to the west, Mungen Taiga Mountain to the north and Kharkhiraa Turgen Mountain to the east (site 1 in Fig. 1) (Sun et al., 2013). The lake exhibits distinct shoreline zonation: low-lying northern/southern margins are salt-marsh vegetation, while the elevated eastern and western shores are dominated by desert steppe communities (Sun et al., 2013). Regional vegetation comprises a mosaic of *Stipa krylovii*, *Stipa gobica* and *Cleistogenes soongorica* grasslands interspersed with shrubs including *Artemisia frigida*, *A. xerophytica*, *A. caespitosa*, *Tanacetum sibiricum*, *T. achillaeoides* and *T. trifidum*. Mountainous areas of the Mongolian Altai host taiga forests dominated by *Larix sibirica* and *P. sibirica* with an understory of *Rosa acicularis* and *Betula rotundifolia* (Sun et al., 2013).

A 2 m sediment core was retrieved from the central lake basin in 2010 using a Livingston-type piston corer (Sun et al., 2013). Five lithological units were identified based on organic matter (OM) content and mean grain size characteristics (Fig. 2A). Ten bulk samples (Table S1) underwent accelerator mass spectrometry (AMS)  $^{14}\text{C}$  dating at the University of Arizona NSF-AMS Facility (Fig. 2A). A 2100-year reservoir correction was applied to all radiocarbon ages prior to calibration due to old carbon-influenced 2099  $^{14}\text{C}$  BP on

the surface sediment and this correction is assumed to be constant throughout the whole sequence (Sun et al., 2013). The calibration to calendar years before present (cal. yr BP, relative to 1950 CE) utilized the IntCal20 curve (Reimer et al., 2020). The Bayesian age-depth model was reconstructed using Bacon v2.5.3 (Blaauw and Christen, 2011) (Fig. 2B) and median ages used to calculate the sedimentation rates in  $\text{yr cm}^{-1}$ . It should be pointed out that we analysed the charcoal data in this study and the pollen and lithology were previously published (Sun et al., 2013). This study just focused on the Holocene interval to investigate the spatial heterogeneities of fire regimes in the Altai-Sayan Mountains and adjacent plains.

## 2.3 Other study sites in the Altai-Sayan Mountains and adjacent plains

A total of 24 sites, including Achit Nuur (Table 1), were selected to investigate the spatial heterogeneity in fire regimes across the Altai-Sayan Mountains and adjacent plains. These sites were divided into seven regions based on the vegetation distribution and geographic location.

Southeastern/western Altai Mountains within steppe zone (Region A,  $n = 4$ ): Tolbo Lake (site 2; 48.55° N, 90.05° E, 2080 m a.s.l.) is an alpine lake of glacial origin covered by mountain steppe in the Mongolian Altai (Hu et al., 2024). Alahake Lake (site 3; 47.69° N, 87.54° E, 483 m a.s.l.) is located in the Irtysh River valley in the southern Altai Mountains (Li et al., 2019). Kuchuk Lake (site 4; 52.69° N,

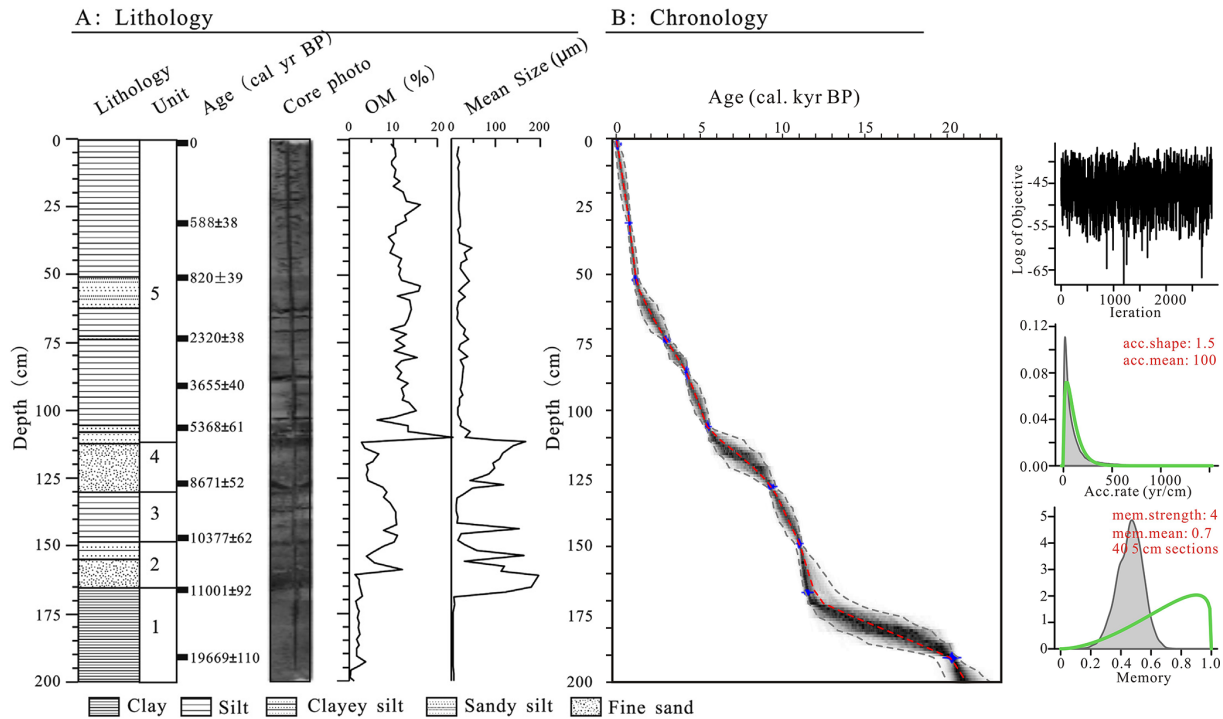


**Figure 2.** Lithology, core photo, organic matter (OM), mean grain size and depth-age model in Achit Nuur (modified from Sun et al., 2013).

79.84° E, 98 m a.s.l.) is the largest endorheic basin in Kurlunda Basin within the southern Siberia (Rudaya et al., 2020).

Low-relief west Siberian plain (Region B,  $n = 4$ ): Rybnaya Mire (site 5; 57.28° N, 84.49° E) is located near the Rybnaya River in the southern taiga of Western Siberia (Feurdean et al., 2022). Plotnikovo Mire (site 6; 56.88° N, 83.30° E, 120 m a.s.l.) is an ombrotrophic bog located at the eastern margins of the Great Vasyugan Mire in Western Siberia (Feurdean et al., 2020). Shchuchye Lake (site 7; 57.13° N, 84.61° E, 80 m a.s.l.) is located in the south taiga zone of the West Siberian plain (Blyakharchuk et al., 2024). Ulukh–Chayakh Mire (site 8; 57.34° N, 88.32° E) is located on a terrace of the Chulym river in the southern taiga of Western Siberia (Feurdean et al., 2022).

Northern Altai Mountains (Region C,  $n = 4$ ): Chudnoye Lake (site 9; 54.03° N, 89.01° E, 1147 m a.s.l.), Tundra Mire (site 10; 53.79° N, 88.27° E, 247 m a.s.l.) and Kuantang Mire (site 12; 51.81° N, 87.32° E, 650 m a.s.l.) are located in the northern Altai Mountains in areas covered by wet mountain dark coniferous (with *Abies*, *P. sibirica* and *Betula*) taiga (Blyakharchuk and Pupysheva, 2022; Blyakharchuk et al., 2024). Mokhovoe Bog (site 11; 52.52° N, 86.42° E, 283 m a.s.l.) is located on the western piedmont of north Altai covered by birch (with *B. pendula* + *B. pubescens*) and pine (*P. sylvestris*) forest-steppe (Blyakharchuk and Pupysheva, 2022).

Central Altai Mountains within the forest zone (Region D,  $n = 3$ ): Dzhangyskol Lake (site 13; 50.18° N, 87.73° E,

1800 m a.s.l.) is situated in the western Kurai intermontane depression covered with steppe vegetation and bounded by small hills with *P. sibirica* and *L. sibirica* (Blyakharchuk et al., 2008). Two freshwater lakes are situated 1.5–4 km apart at different elevations below the timberline in the Ulagan Plateau: Uzunkol Lake (site 14; 50.48° N, 87.1° E, 1985 m a.s.l.) and Kendegelukol Lake (site 15; 50.50° N, 87.63° E, 2050 m a.s.l.) (Blyakharchuk et al., 2004).

Central Altai Mountains above the forest limit (Region E,  $n = 3$ ): Tashkol Lake (site 16; 50.45° N, 87.67° E, 2150 m a.s.l.) lies at the timberline (upper limit of continuous forest) of Ulagan Plateau in the central part of Russian Altai (Blyakharchuk et al., 2004). Akkol Lake (site 17; 50.25° N 89.62° E, 2204 m a.s.l.) and Grusha Lake (site 18; 50.38° N, 89.42° E, 2413 m a.s.l.) are situated in the western Karginskaya high-mountain depression near the junction of the Chikhachev and Shapshal ranges of the south-eastern part of Russian Altai (Blyakharchuk et al., 2007).

Western Sayan Mountains (2000–2700 m a.s.l.) (Region F,  $n = 3$ ): Buibinskoye Mire (site 19; 52.84° N, 93.52° E, 1377 m a.s.l.) and Bezrybnoye Mire (site 20; 52.81° N, 93.50° E, 1395 m a.s.l.) are located in the Yergaki Nature Reserve (Blyakharchuk, 2020). Lugovoe Mire (site 21; 52.85° N, 93.35° E, 1299 m a.s.l.) is the largest mire in the Yergaki Natural Park with the largest hydrological catchment in the Western Sayan Mountains (Blyakharchuk and Chernova, 2013).

**Table 1.** Detailed information of the selected sites across the Altai-Sayan Mountains and adjacent plains.

Region	No.	Site Name	Lat. (N)	Long. (E)	Elev. (m a.s.l.)	Core length (cm)	Time interval (cal. kyr BP)	type of char- coal	References
A	1	Achit Nuur	49.42	90.52	1444	200	22.6	micro	this study
	2	Tolbo Lake	48.55	90.05	2080	253	10.3	micro+	Hu et al. (2025)
	3	Alahake Lake	47.69	87.54	483	140	4.7	micro	Li et al. (2019)
	4	Kuchuk Lake	52.69	79.84	98	255	13.1	macro	Rudaya et al. (2020)
B	5	Rybnaya Mire	57.28	84.49	–	400	8.4	macro	Feurdean et al. (2022)
	6	Plotnikovo Mire	56.88	83.30	120	225	5	macro	Feurdean et al. (2020)
	7	Shchuchye Lake	57.13	84.61	80	331	12.8	micro	Blyakharchuk et al. (2024)
	8	Ulukh–Chayakh Mire	57.34	88.32	–	348	8.5	macro	Feurdean et al. (2022)
C	9	Chudnoye Mire	54.03	89.01	1147	590	12.7	micro	Blyakharchuk et al. (2024)
	10	Tundra Mire	53.79	88.27	247	270	7.28	micro	Blyakharchuk et al. (2024)
	11	Mokhovoe Bog	52.52	86.42	283	638	16.19	micro	Blyakharchuk and Pupysheva (2022)
	12	Kuatang Mire	51.81	87.32	650	557	5.87	micro	Blyakharchuk et al. (2024)
D	13	Dzhangyskol Lake	50.18	87.73	1800	380	13	micro	Blyakharchuk et al. (2008)
	14	Uzunkol Lake	50.48	87.1	1985	285	12.02	micro	Blyakharchuk et al. (2004)
	15	Kendegelukol Lake	50.50	87.63	2050	265	16.01	micro	Blyakharchuk et al. (2004)
E	16	Tashkol Lake	50.45	87.67	2150	205	13.57	micro	Blyakharchuk et al. (2004)
	17	Akkol Lake	50.25	89.62	2204	470	14	micro	Blyakharchuk et al. (2007)
	18	Grusha Lake	50.38	89.42	2413	241	14.37	micro	Blyakharchuk et al. (2007)
F	19	Buibinskoye Mire	52.84	93.52	1377	600	13.11	micro	Blyakharchuk (2020)
	20	Bezrybnoye Mire	52.81	93.50	1395	600	7.23	micro	Blyakharchuk (2020)
	21	Lugovoe Peat	52.85	93.35	1299	330	7.74	micro	Blyakharchuk and Chernova (2013)
G	22	Olgi Lake(OL3)	48.32	98.01	2012	235	9.57	micro	Unkelbach et al. (2021)
	23	Shireet Naiman Nuur	46.53	101.82	2429	178	7.4	micro	Barhoumi et al. (2024)
	24	Uggi Nuur	47.77	102.78	1330	200	22.6	micro	Wang et al. (2011)

Khangai Mountains (peaks 4031 m a.s.l.) (Region G,  $n = 3$ ): Three selected sites include Olgi Lake (site 22; 48.32° N, 98.01° E, 2012 m a.s.l.) (Unkelbach et al., 2021), Shireet Naiman Nuur (site 23; 46.53° N, 101.82° E, 2429 m a.s.l.) (Barhoumi et al., 2024) and Ugii Nuur (site 24; 47.77° N, 102.78° E, 1330 m a.s.l.) (Wang et al., 2011).

### 3 Methods

#### 3.1 Charcoal analysis

The pre-treatment process for charcoal analyses involved the standard pollen extraction method (Tang et al., 2022; Wang et al., 2024). Charcoal particles were identified using a light microscope, characterized by dark black color, opaque appearance, sharp corners, and straight edges. The treated samples were prepared into pollen slides by adding an appropriate amount of glycerin using the particle counting method, which were then observed and counted under a Lycra microscope. A total of more than 300 particles of all sizes were quantified at 400× magnification using an Olympus BX53

microscope and the quantity of Lycopodium spores was determined for each sample.

The concentration of charcoal was calculated based on the statistical data (Li et al., 2024):

$$W = A \times N / (n \times N)$$

where  $W$  is the charcoal concentration (particles  $g^{-1}$ ),  $A$  is the the total count of charcoal fragments,  $n$  is the number of additional lycopodium spores per mount,  $N$  is the statistical number of lycopodium spores, and  $G$  is the sample weight (g). Charcoal influx (CHAR, particles  $cm^{-2} yr^{-1}$ ) is calculated by multiplying the concentration dividing by the sedimentation rate ( $yr cm^{-1}$ ) derived from the age-depth model (see Sect. 2.2).

#### 3.2 Generalized additive models

Generalized additive models (GAMs) employ a link function to examine the relationship between the mean of the response variable (i.e., dependent variable) and a smoothed function of the predictor variable (i.e., independent variable).

The model convergence and adequacy were assessed using the `gam.check()` function in R and confirmed that the basis dimensions ( $k$ ) were sufficient and inspected diagnostic plots of residuals to ensure the model structure was appropriate. In this study, we investigated the associations between charcoal influx and two types of predictors: (1) individual taxa, including *Abies*, *Betula*, *Larix*, *Picea*, *P. sibirica* and *P. sylvestris*, because they represent the dominant arboreal species in the study area and are key components of the regional forest ecosystems; and (2) total forest cover, defined as the summed percentage of the aforementioned six taxa.

We constructed GAMs with a quasi-Poisson distribution and a log link function using the `mgcv` package in R (Wood, 2017). This distribution was selected because it flexibly corrects for overdispersion without requiring a specific parametric distribution for the data (Wood, 2017). For all smoothing terms, we used thin-plate splines as the basis function – this is the default setting in the `gam()` function of the `mgcv` package. The model fitting was performed via restricted maximum likelihood (REML) for smoothness selection.

### 3.3 Data processing for comparison

To render charcoal influx records from different sites comparable, a three-step transformation procedure was applied to calculate comparable  $Z$ -scores (Power et al., 2007):

1. Min-max transformation: Raw influx values were rescaled to a 0–1 range to reduce the influence of varying magnitudes between sites.

$$C_i' = (C_i - C_{\min}) / (C_{\max} - C_{\min})$$

In this expression,  $C_i'$  is the value of mini-max transformed for the  $i$ th sample at each sequence,  $C_i$  is the charcoal influx (CHAR) value for the  $i$ th sample at each sequence,  $C_{\max}$  is the maximum value of  $C_i$ , and  $C_{\min}$  is the minimum value of  $C_i$ .

2. Box-Cox transformation for homogenization of variance: This transformation was applied to homogenize within-record variance and improve the normality of the data distribution, satisfying the assumptions for subsequent statistical analyses.

$$C_i^* = \begin{cases} ((C_i' + \alpha)^\lambda - 1) / \lambda, & \lambda \neq 0 \\ \log(C_i' + \alpha), & \lambda = 0 \end{cases}$$

In this expression,  $C_i^*$  is the Box-Cox value transformed for  $C_i'$ ,  $\lambda$  is the parameter of Box-Cox transformation estimated using maximum likelihood, and  $\alpha$  is a small constant added to ensure all data values are positive ( $> 0$ ) prior to the Box-Cox transformation, as the function cannot handle zero values.

3.  $Z$ -score calculation: The transformed data were converted into  $Z$ -scores (standardized anomalies with a

mean of 0 and unit variance) to facilitate direct comparison and the synthesis of charcoal records across different sites.

$$Z\text{-score} = (C_i^* - \overline{C_i^*}) / \delta$$

In this expression,  $\overline{C_i^*}$  is the average value of  $C_i^*$  and  $\delta$  is the standard deviation of  $C_i^*$ .

Considering the  $\sim 200$ -year sample resolution at most sites, the transformed  $Z$ -scores were linearly interpolated to 200-year time steps. Subsequently, the interpolated data were averaged using a binning method to construct composite curves that characterize fire regimes across different regions. The Holocene interval was divided into three intervals: early Holocene ( $\sim 11.75$ – $\sim 8.2$  cal. kyr BP), middle Holocene ( $\sim 8.2$ – $\sim 4.2$  cal. kyr BP) and late Holocene ( $\sim 4.2$ – $\sim 0$  cal. kyr BP) (Marcott et al., 2013).

## 4 Results and Discussions

### 4.1 Reconstructed fire history and its relationship with vegetation at Achit Nuur

The charcoal influx in Achit Nuur varies from 67 to 2643 particles  $\text{cm}^{-2} \text{yr}^{-1}$  with an average of 501 particles  $\text{cm}^{-2} \text{yr}^{-1}$ . Notably, higher charcoal influx has been recorded since  $\sim 2$  cal. kyr BP with the maximum occurring during the interval of  $\sim 1.2$ – $\sim 0.79$  cal. kyr BP (Fig. 3a). Regarding pollen trends: *P. sibirica*, *Betula* and *Picea* exhibited a rapid increase before  $\sim 6$  cal. kyr BP, followed by a gradual decreasing trend (Fig. 3b) (Sun et al., 2013). High *Larix* pollen content was observed from  $\sim 6$  to  $\sim 2$  cal. kyr BP, while *Abies* pollen remained relatively low throughout the entire sequence. GAMs analyses reveal charcoal influx is significantly positively correlated with the abundance of *Betula* (Deviance explained = 20%,  $p = 0.02$ ), *P. sibirica* (Deviance explained = 34.5%,  $p = 0.001$ ) and total forest cover (Deviance explained = 41.5%,  $p < 0.001$ ). Conversely, it is significantly negatively correlated with decreasing *Larix* (Deviance explained = 41.9%,  $p < 0.001$ ) and *Picea* (Deviance explained = 19.2%,  $p = 0.001$ ) abundances (Table 2, Fig. 1).

The strong positive relationship between charcoal and forest cover suggests that this region functions as a fuel-limited system, where biomass availability regulates fire activities. Mechanistically, the late-Holocene fire increase coincides with a shift in vegetation composition: the decline of *Larix* (often a fire-avoidant species that maintains moister sub-canopy conditions) after  $\sim 2$  cal. kyr BP likely increased landscape flammability. In contrast, taxa such as *Betula* and *P. sibirica* possess traits like thinner bark and more resinous tissues (Feurdean et al., 2020, 2022) that facilitate fire spread and intensity. Thus, these shifts in relative species directly regulated the observed variation in charcoal influx.

**Table 2.** Correlation between the independent variables represented by pollen percentages (*Abies*, *Betula*, *Larix*, *Picea*, *Pinus sibirica*, *Pinus sylvestris* and their sum (i.e., forest cover) and the dependent variable (charcoal influx). The significance of each parameter is given by  $p$  values where \*\*\*  $p < 0.001$ ; \*\*  $p < 0.01$ ; \*  $p < 0.05$ .

Site Name	Independent variable	edf	ref.df	$F$ value	$p$ -value	Deviance explained
Achit Nuur	<i>Abies</i>	–	–	–	–	–
	<i>Betula</i>	2.75	3.47	3.40	0.02*	21 %
	<i>Larix</i>	3.51	4.21	8.72	0.00***	41.9 %
	<i>Picea</i>	1	1	11.36	0.001**	19.2 %
	<i>Pinus sibirica</i>	2.73	3.41	5.70	0.001**	34.5 %
	<i>Pinus sylvestris</i>	–	–	–	–	–
	Forest cover	2.92	3.69	8.02	0.00***	41.5 %
Tolbo Lake	<i>Abies</i>	–	–	–	–	–
	<i>Betula</i>	6.96	8.01	1.76	0.09	7.04 %
	<i>Larix</i>	1.03	1.07	0.03	0.95	0.03 %
	<i>Picea</i>	2.97	3.75	4.47	0.002**	8.11 %
	<i>Pinus sibirica</i>	2.68	3.39	9.55	0.00***	13.3 %
	<i>Pinus sylvestris</i>	–	–	–	–	–
	Forest cover	2.98	3.75	8.96	0.00***	14.3 %
Alahake Lake	<i>Abies</i>	1	1	0.57	0.45	1.1 %
	<i>Betula</i>	1	1	4.19	0.04*	5.2 %
	<i>Larix</i>	6.85	7.94	1.42	0.19	11.6 %
	<i>Picea</i>	3.84	4.77	1.96	0.09	10 %
	<i>Pinus sibirica</i>	5.59	6.77	1.85	0.09	13 %
	<i>Pinus sylvestris</i>	–	–	–	–	–
	Forest cover	2.17	2.77	1.24	0.26	5.07 %
Kuchuk Lake	<i>Abies</i>	1.21	1.40	3.80	0.03*	9.81 %
	<i>Betula</i>	1.38	1.67	16.18	0.00***	25.2 %
	<i>Larix</i>	1.11	1.21	0.01	0.98	0.19 %
	<i>Picea</i>	1.16	1.30	1.31	0.30	2.29 %
	<i>Pinus sibirica</i>	5.84	6.89	1.06	0.39	9.51 %
	<i>Pinus sylvestris</i>	6.54	7.64	2.61	0.01*	25.5 %
	Forest cover	3.59	4.47	1.22	0.28	11 %
Rybnaya Mire	<i>Abies</i>	5.28	6.31	1.99	0.07	11.7 %
	<i>Betula</i>	4.90	6.00	3.32	0.004**	18.4 %
	<i>Larix</i>	7.07	8.11	1.95	0.07	20.6 %
	<i>Picea</i>	8.15	8.79	14.1	0.00***	44.5 %
	<i>Pinus sibirica</i>	6.74	7.86	1.68	0.12	16.6 %
	<i>Pinus sylvestris</i>	2.03	2.54	1.06	0.35	4 %
	Forest cover	7.00	8.10	3.06	0.003**	16.2 %
Plotnikovo Mire	<i>Abies</i>	3.12	3.88	0.70	0.55	16.7 %
	<i>Betula</i>	2.69	3.36	1.40	0.26	19.6 %
	<i>Larix</i>	1	1	4.09	0.06	20.1 %
	<i>Picea</i>	2.12	2.65	1.54	0.26	15.1 %
	<i>Pinus sibirica</i>	1.68	2.11	0.41	0.7	4.85 %
	<i>Pinus sylvestris</i>	2.01	2.53	1.50	0.23	14.7 %
	Forest cover	4.43	5.21	4.07	0.004**	39.7 %
Schuchye Lake	<i>Abies</i>	4.78	5.85	5.39	0.00***	37.4 %
	<i>Betula</i>	1	1	5.29	0.03*	10.8 %
	<i>Larix</i>	1	1	63.71	0.00***	45.4 %
	<i>Picea</i>	2.19	2.71	3.77	0.02*	17.5 %
	<i>Pinus sibirica</i>	1	1	27.6	0.00***	30.8 %
	<i>Pinus sylvestris</i>	3.15	3.90	3.31	0.02*	21.2 %
	Forest cover	2.10	2.52	7.91	0.00***	24.7 %

Table 2. Continued.

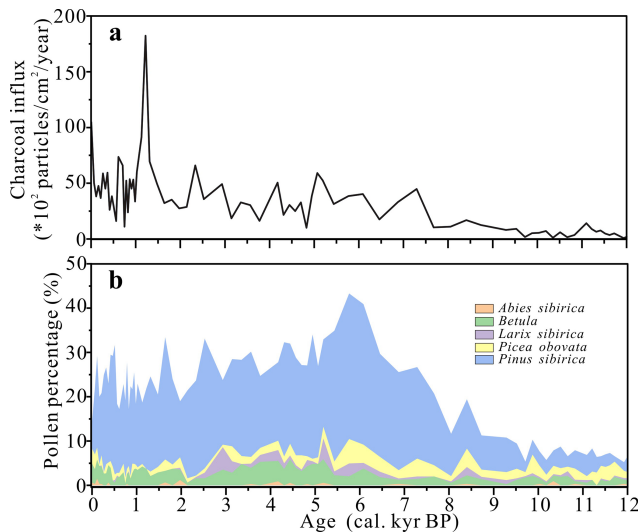
Site Name	Independent variable	edf	ref.df	F value	p-value	Deviance explained
Ulukh–Chayakh Mire	<i>Abies</i>	6.38	7.52	1.60	0.18	29.4 %
	<i>Betula</i>	1	1	6.44	0.01*	13.4 %
	<i>Larix</i>	2.54	3.16	2.46	0.07	17.5 %
	<i>Picea</i>	2.45	3.12	1.46	0.23	16.7 %
	<i>Pinus sibirica</i>	1	1	0.66	0.42	1.82 %
	<i>Pinus sylvestris</i>	1	1	4.43	0.04*	10.3 %
	Forest cover	4.26	5.08	1.46	0.22	16.9 %
Chudnoye Lake	<i>Abies</i>	1.75	2.17	2.09	0.14	8.52 %
	<i>Betula</i>	1.23	1.42	10.54	0.001**	23.5 %
	<i>Larix</i>	2.06	2.57	3.84	0.03*	14.7 %
	<i>Picea</i>	1.99	2.44	11.76	0.00***	30.3 %
	<i>Pinus sibirica</i>	4.33	5.25	3.38	0.01*	26.6 %
	<i>Pinus sylvestris</i>	1	1	6.59	0.01*	11.6 %
	Forest cover	1	1	1.97	0.17	3.5 %
Tundra Mire	<i>Abies</i>	2.16	2.75	0.78	0.57	3.83 %
	<i>Betula</i>	1	1	3.27	0.07	4.44 %
	<i>Larix</i>	6.41	7.35	4.32	0.00***	22.7 %
	<i>Picea</i>	1	1	0.09	0.77	0.13 %
	<i>Pinus sibirica</i>	2.39	2.99	0.83	0.46	4.66 %
	<i>Pinus sylvestris</i>	3.03	3.78	0.79	0.49	5.83 %
	Forest cover	1	1	2.79	0.10	3.53 %
Mokhove Bog	<i>Abies</i>	1.83	2.31	1.12	0.38	3.65 %
	<i>Betula</i>	6.81	7.88	2.07	0.05	17.2 %
	<i>Larix</i>	1.09	1.17	0.24	0.63	0.59 %
	<i>Picea</i>	2.59	3.22	3.54	0.02*	11.9 %
	<i>Pinus sibirica</i>	1	1	0.00	0.96	0.003 %
	<i>Pinus sylvestris</i>	4.46	5.49	1.78	0.11	13 %
	Forest cover	5.04	6.19	0.91	0.48	10.3 %
Kuatang Mire	<i>Abies</i>	2.45	3.14	2.78	0.04*	13.8 %
	<i>Betula</i>	1	1	29.13	0.00***	24.5 %
	<i>Larix</i>	1	1.00	0.06	0.81	0.08 %
	<i>Picea</i>	6.72	7.79	1.19	0.31	13.4 %
	<i>Pinus sibirica</i>	1.43	1.74	2.92	0.05*	6.90 %
	<i>Pinus sylvestris</i>	1	1	5.83	0.02*	6.51 %
	Forest cover	1	1	9.24	0.003**	10.9 %
Dzhangyskol Lake	<i>Abies</i>	3.64	4.53	0.45	0.79	16.9 %
	<i>Betula</i>	1.79	2.23	0.37	0.77	7.12 %
	<i>Larix</i>	1	1	0.05	0.83	0.33 %
	<i>Picea</i>	3.92	4.80	0.82	0.51	24.8 %
	<i>Pinus sibirica</i>	1.70	2.12	0.35	0.73	7.06 %
	<i>Pinus sylvestris</i>	3.05	3.75	1.22	0.29	22.8 %
	Forest cover	2.39	3.04	0.67	0.58	15.6 %
Uzunkol Lake	<i>Abies</i>	1	1	5.329	0.02*	7.04 %
	<i>Betula</i>	4.92	5.99	3.22	0.01**	29.4 %
	<i>Larix</i>	1	1	14.38	0.00***	22.1 %
	<i>Picea</i>	5.99	7.12	5.03	0.00***	40.1 %
	<i>Pinus sibirica</i>	2.04	2.57	1.99	0.14	14.7 %
	<i>Pinus sylvestris</i>	4.79	5.81	2.85	0.02*	29.3 %
	Forest cover	2.17	2.69	1.39	0.27	14.2 %

Table 2. Continued.

Site Name	Independent variable	edf	ref.df	F value	p-value	Deviance explained
Kendegelukol Lake	<i>Abies</i>	4.93	5.97	2.63	0.04*	41.4 %
	<i>Betula</i>	5.87	7.04	2.78	0.02*	49.4 %
	<i>Larix</i>	1	1	3.11	0.09	9.63 %
	<i>Picea</i>	2.99	3.73	2.19	0.08	29.4 %
	<i>Pinus sibirica</i>	2.25	2.78	2.26	0.09	28.9 %
	<i>Pinus sylvestris</i>	1	1	18.48	0.00***	40 %
	Forest cover	1.57	1.91	3.58	0.06	26.9 %
Tashkol Lake	<i>Abies</i>	1	1	0.02	0.90	0.09 %
	<i>Betula</i>	1	1	0.08	0.79	0.36 %
	<i>Larix</i>	1.56	1.92	0.20	0.82	3.52 %
	<i>Picea</i>	6.69	7.81	2.35	0.04*	40.7 %
	<i>Pinus sibirica</i>	1	1	0.004	0.95	0.02 %
	<i>Pinus sylvestris</i>	1	1	0.02	0.89	0.09 %
	Forest cover	3.00	3.75	0.90	0.48	17 %
Akkol Lake	<i>Abies</i>	1.76	2.11	0.79	0.43	4.83 %
	<i>Betula</i>	1	1	0.96	0.33	1.76 %
	<i>Larix</i>	6.53	7.59	1.94	0.08	30.4 %
	<i>Picea</i>	2.41	3.03	6.77	0.00***	31.6 %
	<i>Pinus sibirica</i>	4.35	5.41	1.90	0.1	23 %
	<i>Pinus sylvestris</i>	1	1	10.12	0.002**	18.9 %
	Forest cover	8.47	8.92	5.49	0.00***	55.1 %
Grusha Lake	<i>Abies</i>	1	1	0.62	0.44	2.75 %
	<i>Betula</i>	1	1	0.88	0.36	3.93 %
	<i>Larix</i>	3.81	4.58	3.44	0.02*	49.3 %
	<i>Picea</i>	2.18	2.71	3.30	0.05*	35.80 %
	<i>Pinus sibirica</i>	1	1	0.60	0.45	2.67 %
	<i>Pinus sylvestris</i>	1.39	1.66	0.19	0.76	4.67 %
	Forest cover	2.55	3.18	12.7	0.00***	71.1 %
Bezrybnoe Mire	<i>Abies</i>	1.15	1.29	0.31	0.75	1.16 %
	<i>Betula</i>	1.74	2.20	1.63	0.22	8.85 %
	<i>Larix</i>	2.58	3.14	0.32	0.79	4.76 %
	<i>Picea</i>	1	1	2.13	0.15	4.49 %
	<i>Pinus sibirica</i>	1.37	1.66	0.39	0.75	2.18 %
	<i>Pinus sylvestris</i>	6.47	7.53	1.69	0.13	28.1 %
	Forest cover	1	1	0.01	0.93	0.02 %
Buibinskoye Mire	<i>Abies</i>	2.71	3.39	4.85	0.004**	29.6 %
	<i>Betula</i>	2.11	2.69	2.29	0.10	17.4 %
	<i>Larix</i>	1	1	1.16	0.29	2.83 %
	<i>Picea</i>	1.52	1.87	0.71	0.40	4.85 %
	<i>Pinus sibirica</i>	2.02	2.57	2.70	0.05	17.4 %
	<i>Pinus sylvestris</i>	1	1	3.78	0.06	7.42 %
	Forest cover	3.61	4.42	2.47	0.06	22.6 %
Lugovoe Mire	<i>Abies</i>	1	1	6.32	0.02*	15.3 %
	<i>Betula</i>	1	1	0.23	0.64	0.79 %
	<i>Larix</i>	5.00	5.91	3.89	0.01**	43.5 %
	<i>Picea</i>	4.00	4.95	2.41	0.07	35.8 %
	<i>Pinus sibirica</i>	3.43	4.28	2.20	0.09	31 %
	<i>Pinus sylvestris</i>	8.81	8.98	3.21	0.01*	60.5 %
	Forest cover	1.14	1.27	0.20	0.67	2.29 %

Table 2. Continued.

Site Name	Independent variable	edf	ref.df	F value	p-value	Deviance explained
Olgi Lake	<i>Abies</i>	–	–	–	–	–
	<i>Betula</i>	4.89	5.96	2.91	0.02*	34.5 %
	<i>Larix</i>	4.32	5.29	2.68	0.03*	35.6 %
	<i>Picea</i>	3.8	4.65	4.20	0.003**	35.7 %
	<i>Pinus sibirica</i>	8.62	8.89	45.23	0.00***	27.9 %
	Forest cover	–	–	–	–	–
Shireet Naiman Nuur	<i>Abies</i>	–	–	–	–	–
	<i>Betula</i>	2.57	3.211	3.82	0.01*	20.7 %
	<i>Larix</i>	1	1	1.59	0.21	2.83 %
	<i>Picea</i>	1	1	6.55	0.01*	9.70 %
	<i>Pinus sibirica</i>	3.98	4.91	4.02	0.003**	27.5 %
	<i>Pinus sylvestris</i>	1	1	7.99	0.01**	12 %
Forest cover	4.01	4.96	6.38	0.00***	37.4 %	
Uggi Nuur	<i>Abies</i>	–	–	–	–	–
	<i>Betula</i>	6.49	7.59	2.02	0.06	8.65 %
	<i>Larix</i>	6.48	0.06	104.4	0.00***	12.2 %
	<i>Picea</i>	1	1	0.18	0.67	0.1 %
	<i>Pinus sibirica</i>	8.55	8.94	6.19	0.00***	19.4 %
	<i>Pinus sylvestris</i>	–	–	–	–	–
Forest cover	8.07	8.76	5.72	0.00***	18.4 %	



**Figure 3.** Achit Nuur: charcoal influx (a) and vegetation change (b) (Sun et al., 2013; this study).

## 4.2 Holocene climate-fuel feedbacks across selected sites

### 4.2.1 Southeastern/western Altai Mountains within the steppe zone (Region A)

Charcoal records from four lacustrine systems (Achit Nuur, Tolbo, Alahake and Kuchuk Lakes) reveal a consistent

amplification of fire activity during the late- Holocene (Fig. 4b). Distinct peak intervals vary across sites:  $\sim 1.2$ – $\sim 0.79$  cal. kyr BP at Achit Nuur,  $\sim 1.20$ – $\sim 0.65$  cal. kyr BP at Tolbo Lake,  $\sim 1.44$ – $\sim 1.02$  cal. kyr BP at Alahake Lake, and a pronounced doubling of charcoal flux over the past two millennia at Kuchuk Lake. Pollen spectra highlight the ecosystem-specific fuel configurations that underpin these fire patterns: Tolbo Lake is dominated by an alpine steppe ecosystem (*Artemisia*-*Poaceae*), where herbaceous plants serve as the primary surface fuel; Achit Nuur features montane *P. sibirica* providing highly flammable resinous fuel sources. Alahake Lake is surrounded by lowland *Picea*-*Larix* mixed forest, where leaf litter and understory vegetation contribute to fuel loads (Sun et al., 2013; Hu et al., 2024; Li et al., 2019; Rudaya et al., 2020).

This divergence in fuel strategy explains the varied fire responses to environmental changes. GAMs analyses confirm that charcoal influx at Achit Nuur and Tolbo Lake is primarily controlled by forest cover (Table 2, Fig. S1, Sect. S1 in the Supplement). Specifically, *Larix* (41.9 % deviance explained) and *P. sibirica* (34.5 %) are key drivers in Achit Nuur, whereas *P. sibirica* (13.3 %) plays a dominant role at Tolbo Lake. At Alahake Lake, *Betula* (with its thin bark and volatile leaf litter) is the primary combustion source. Notably, at Kuchuk Lake, the post-2 cal. kyr BP doubling of charcoal influx is explicitly linked to the expansion of *Betula* and *P. sylvestris* forest – both of which possess high ignition potential (Table 2, Fig. S2).

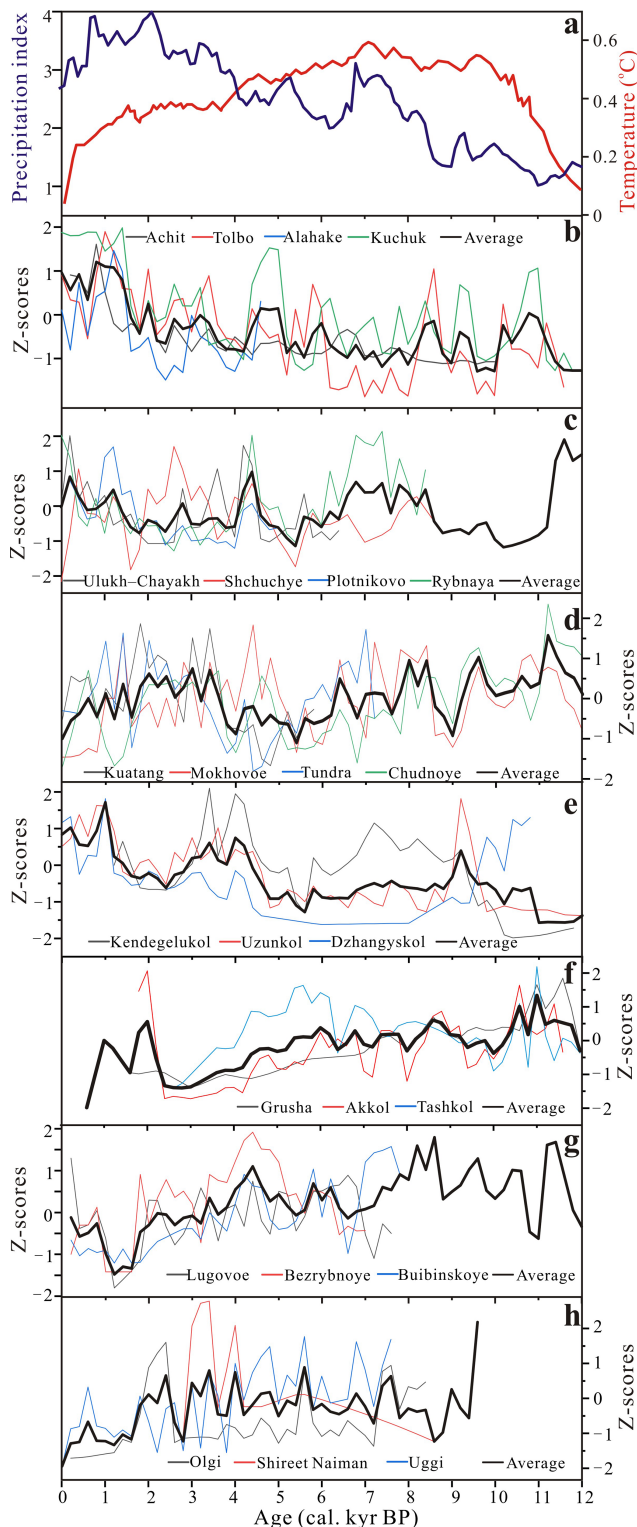


**Figure 4.** Regional integrated charcoal influx (b–g) under the context of temperature (Marcott et al., 2013) and precipitation index (a) in the Holocene interval (Zhang and Feng, 2018).

#### 4.2.2 West Siberian plain (Region B, $n = 4$ )

Rybnaya Mire, located on the low terrace of the Ob' River (83 m a.s.l.) and dominated by *P. sylvestris* and *Betula*, shows higher influx during the middle Holocene but no significant charcoal pulse over the past 50 years (Feurdean et al., 2020) (Fig. 4c). GAM analysis indicates fire activity is primarily controlled by coniferous vegetation with *Picea* abundance explaining 44.5 % of the variance (Table 2, Fig. S2). In contrast, Plotnikovo Mire exhibits a rapid charcoal increase since  $\sim 2$  cal. kyr BP (Feurdean et al., 2020). This surge is likely linked to the gradual expansion of *Betula* (forest cover explaining 39.7 % of deviance) (Table 2, Fig. S2, Sect. S1), as the accumulation of its flammable resinous bark created more favorable conditions for fire ignition and spread (Feurdean et al., 2022). Shchuchye Lake displays a phased fire regime, marked by a strong charcoal pulse at the Younger Dryas–Early Holocene transition ( $\sim 12$ – $\sim 11$  cal. kyr BP) and slightly increased fire activity during the late Holocene (Fig. 4c). Ulukh-Chayakh Mire records key fire events in the last millennium and during the  $\sim 4.5$ – $\sim 3$  cal. kyr BP interval (Fig. 4c).

GAM analyses reveal the divergent fire-vegetation relationships rooted in canopy structure (Table 2, Figs. S2 and S3, Sect. S1): (1) Negative correlation at Rybnaya and Plotnikovo Mires (canopy cover  $> 75$  %): Dense canopies limit light availability, maintaining humid microclimatic that suppress the herbaceous understory growth. This creates moist surface conditions and sparse fine fuels, resulting in an inverse relationship between canopy cover and fire. (2) Positive correlation at Shchuchye Lake (canopy cover  $< 65$  %): Open canopy structures allow solar radiation to reach the forest floor, promoting the growth of flammable grassy understories. These fine fuels dry quickly and ignite easily, while the open environment facilitates air circulation and fire spread, leading to a positive association between canopy openness and charcoal influx.

#### 4.2.3 Northern Altai Mountains (Region C, $n = 4$ )

Chudnoye Mire, situated in a remote mountain taiga near the upper forest limit (Fig. 1), exhibits a decline in influx during the early to mid-Holocene followed by late Holocene intensification (Fig. 4d). This variations correlates positively with *Betula* (30.3 %) and *Picea* (20.5 %) abundances (Table 2, Fig. S3, Sect. S1). The mechanism lies in pyroptic properties of these taxa (*Betula* and *Picea*): their needle litter and resinous tissues that are highly flammable when dry, directly boosting fire frequency (Blyakharchuk et al., 2024).

Tundra Mire, characterized by dense forests of *Abies* and *Betula*, shows rising charcoal influx after  $\sim 4$  cal. kyr BP. GAM analysis suggests that this trend stems from the fire-adapted traits of *Larix* (22.7 % of deviance explained) (Table 2, Fig. S4). Mokhovoe Bog, a birch forest-steppe site, records four charcoal influx peaks at  $\sim 11.5$ – $\sim 9.5$ ,

~ 8.5–~7, ~ 5.6–~4 and ~ 1.5–~1 cal. kyr BP. A statistical correlation (11.9%) with *Picea* pollen (Table 2, Fig. S4) suggests a climatic controls on fuel production: humid conditions enhance bioproductivity and litter accumulation. Although *Picea* is less flammable than *Betula*, the sheer increase in fuel loads drives higher charcoal influx (Blyakharchuk and Pupysheva, 2022).

Kuatang Lake shows a clear charcoal increase between ~ 3.5 and ~ 2 cal. kyr BP (Figs. 4d, S4). A distinct vegetation-fire pattern emerges here: charcoal influx positively correlated with *Betula* pollen but negatively with *Abies*, *P. sibirica* and *P. sylvestris*. This suggests that the post-3.5 cal. kyr BP fire increase was driven by the expansion of fire-prone *Betula* (thin, volatile bark) at the expense of more fire-resistant conifers (thick bark, dense canopies) (Blyakharchuk et al., 2024).

#### 4.2.4 Central Altai Mountains within the forest zone (Region D, $n = 3$ )

Charcoal influx exhibited a consistent increasing trend across Kendegelukol Lake, Uzunkol Lake and Dzhangyskol Lake (Fig. 4e), with pronounced acceleration during the late Holocene. Uzunkol Lake records a sharp rise in charcoal influx since ~ 1.2 cal. kyr BP, while Dzhangyskol Lake increases markedly from ~ 0.5 cal. kyr BP onward. Notably, Uzunkol Lake also documented elevated charcoal influx between ~ 9.5 and ~ 9 cal. kyr BP, coinciding with the steppe-to-forest transition (Blyakharchuk et al., 2008). This early Holocene peak likely arose from an unstable fire regime during the forest establishment: dry climatic conditions combined with increasing woody fuel loads made the nascent ecosystem highly susceptible to ignition (Blyakharchuk and Pupysheva, 2022). The subsequent landscape stabilization and humidification suppressed fire activity until the late Holocene (Zhang and Zhang, 2025).

Kendegelukol Lake and Dzhangyskol Lake exhibited modest increases in charcoal influx throughout the Holocene (Fig. 4e). This contrast highlights Uzunkol Lake's sensitivity as an ecotone site (Blyakharchuk et al., 2004). Located in the forest-steppe transition zone, its dynamic vegetation mix is highly responsive to minor climatic fluctuations, amplifying fire signals. In contrast, the cohesive forests at these two sites buffer against small-scale environmental changes (Lezine et al., 2023). GAM analyses across all three lakes reveal strong positive correlations with *Abies*, *Betula* and *P. sylvestris* (Table 2, Fig. S5, Sect. S1), confirming that the late-Holocene forest expansion enhanced fuel accumulation, thereby lowering ignition thresholds.

#### 4.2.5 Central Altai Mountains above the forest limit (Region E, $n = 3$ )

Tashkol Lake (2150 m a.s.l.) exhibits a sharp peak in charcoal influx at ~ 11–~ 10.5 cal. kyr BP, likely caused

by a paraglacial mechanism: meltwaters redeposition of Pleistocene-aged microcharcoal following deglaciation (Blyakharchuk et al., 2004, 2024). Subsequently, the middle Holocene warming (~ 10.5–~ 4 cal. kyr BP) promoted high-elevation expansion, increasing biomass and charcoal influx via a temperature-dependent mechanism. Late Holocene cooling reversed this trend.

Grusha Lake (2413 m a.s.l.) shows a similar pattern with an exceptionally late-glacial (~ 12–~ 11 cal. kyr BP) high charcoal influx attributed to the allochthonous redeposition (Rudoy and Yatsuk, 1986; Blyakharchuk et al., 2024). Following deglaciation (~ 10.5 cal. kyr BP), vegetation colonization stabilized the landscape, shifting the record to reflect in-situ fire activity (Blyakharchuk et al., 2004). Akkol Lake mirrors the general trend but lacks the ~ 12–~ 11 cal. kyr BP peak. This absence is explained by its lower elevation and lack of glacial coverage during the last glaciation (Blyakharchuk et al., 2007). Without glaciers to accumulate ancient microcharcoal, and with drier conditions inhibiting sediment transport, Akkol Lake records only minimal in-situ fire activity during this period.

GAMs analyses identify the key vegetation sources of biomass combustion across three lakes: *Picea* (40.7%) in Tashkol Lake; a combination of *Picea* (31.6%) and *Larix* (30.4%) in Akkol Lake; and *Larix* (49.3%) and *Picea* (35.80%) in Grusha Lake (Table 2, Fig. S6, Sect. S1). These species-specific associations reflect differences in fuel flammability – *Larix* produce resin-rich needles and bark that ignite easily, while *Picea* litter, though less flammable, contributes to fuel loads when accumulated in large quantities (Blyakharchuk et al., 2004) – ultimately driving lake-specific variations in charcoal influx. Notably, significant differences in charcoal influx magnitudes and timing were observed among three lakes, largely tied to their distinct elevations, glacial histories and post-glacial vegetation development.

#### 4.2.6 Western Sayan Mountains (Region F, $n = 3$ )

Records from Lugovoe Peat, Bezrybnoye Mire and Buibinskoye Mire generally show decreasing Holocene charcoal records. A notable exception is the ~ 12–~ 11 cal. kyr BP peak at Buibinskoye Mire (Fig. 4g). As permafrost receded and the region transitioned from cold, waterlogged soils supporting sparse *Picea* to better-drained substrates, *P. sibirica* and *Abies* expanded (Blyakharchuk, 2020; Blyakharchuk and Chernova, 2013). The ~ 11 cal. kyr BP peak reflects this forestation event. A transient warming just prior (~ 11.5–~ 11 cal. kyr BP) likely dried sparse spruce litter, triggering intense fires. Following a mid-Holocene maximum (~ 10.5–~ 7 cal. kyr BP) driven by warming-enhanced productivity, charcoal influx declined as late-Holocene cooling reduced fuel accumulation.

GAMs results highlight species-specific roles in driving charcoal influx: in Lugovoe Peat, *Abies* and *Larix* are

the primary contributor to charcoal production. However, at Bezrybnoye Mire, fire-resistant *P. sylvestris* explains the most variance (28.10 %) (Table 2, Fig. S7, Sect. S1). This suggests a negative feedback: the expansion of *P. sylvestris* displaced more flammable taxa, reducing overall forest flammability and driving the long-term decline in charcoal influx.

#### 4.2.7 Khangai Mountains (Region G, $n = 3$ )

At Olgi Lake, a negative correlation (33.3 %) between charcoal influx and primary forest cover suggests fires are fueled by steppe herbs (Table 2, Fig. S8). An decrease in forest cover would promote grass-fueled fires, leading to higher charcoal influx – explaining the observed negative correlation (Sun et al., 2013). Conversely, at Shireet Naiman Nuur (37.4 %) and Ugii Nuur (18.4 %), positive correlations with forest cover (especially *P. sibirica*) (Table 2, Fig. S8) indicate woody biomass drives fire activity. Despite similar trends, Shireet Naiman Nuur records lower overall influx due to elevation-limited productivity (Barhoumi et al., 2024).

Marked charcoal spikes were recorded at at Olgi Lake ( $\sim 3.4\text{--}3.1$  cal. kyr BP) and Ugii Nuur ( $\sim 2.4\text{--}2.1$  cal. kyr BP), which align with periods of local drought (Unkelbach et al., 2021; Barhoumi et al., 2024; Wang et al., 2011). In the absence of significant human impact during these intervals, drought likely acted as a natural catalyst, drying fuels and increasing susceptibility to ignition.

### 4.3 Holocene climate-fuel feedbacks across the different regions

In Region A, fire activity was suppressed during the dry early Holocene due to limited fuel availability (Zhang and Zhang, 2025; Sun et al., 2013; Hu et al., 2024; Li et al., 2019; Rudaya et al., 2020). From the mid-Holocene to  $\sim 2$  cal. kyr BP, increased precipitation (Hu et al., 2024; Zhang and Zhang, 2025) facilitated vegetation expansion, fueling a gradual rise in fires. Crucially, after  $\sim 2$  cal. kyr BP, anomalous charcoal peaks across all sites correlate with pollen evidence of agricultural expansion (e.g., cereal-type Poaceae; Xiao et al., 2021). This synchrony suggests that anthropogenic disturbances – specifically intentional burning for pasture and crop management – overrode climatic controls to become the dominant driver of fire frequency (Li et al., 2019; Xiao et al., 2021; Rudaya et al., 2020).

In Region B, fire history divides into three phases: (1) An early pulse ( $\sim 12\text{--}11$  cal. kyr BP) at Shchuchye Lake driven by paraglacial processes (Blyakharchuk et al., 2024); (2) A mid-Holocene increase ( $\sim 8.5\text{--}6$  cal. kyr BP) at Rybnaya Peat linked to the expansion of dark taiga (Feurdean et al., 2022); and (3) A widespread fire surge past  $\sim 2$  cal. kyr BP. This late-Holocene intensification resulted from the synergistic effects of megadrought conditions (dry-

ing vegetation) and the emergence of pastoralist fire use (Feurdean et al., 2022).

In Region C, a late-Holocene increase in fire activity (following an early-Holocene decline) correlates with regional humidification and intensified human occupation (Blyakharchuk et al., 2023; Zhang and Zhang, 2025). While moisture increased biomass, human activities provided ignition sources. Notably, charcoal pulses in the Bronze Age ( $\sim 4\text{--}3$  cal. kyr BP) and Early Iron Age ( $\sim 3$  cal. kyr BP) coincide with metallurgical centers in the Kuznetski Alatau (Slavnin and Sherstova, 1999), linking fire history directly to cultural expansion (Panyushkina, 2012; Agatova et al., 2016; Xiang et al., 2023; Blyakharchuk and Pupysheva, 2022; Slavnin and Sherstova, 1999).

In Region D, a 2.3-fold increase in charcoal influx over the last two millennia (Fig. 4e) reflects the cumulative impact of forest expansion (natural fuel buildup) and pastoral burning. The sharp rise after  $\sim 1.0$  cal kyr BP, in particular, points to intensified land clearance and management by pastoralists, which altered vegetation structure and amplified flammability (Zhang et al., 2022; Blyakharchuk et al., 2004, 2008).

In Regions E and F, long-term trends differ mainly by vegetation trajectory. In Region E, temperature-driven (Blyakharchuk et al., 2007) forest fluctuations dictated fuel loads (Fig. 4f), with a late anthropogenic overprint. In Region F, the progressive expansion of fire-resistant *P. sylvestris* caused a long-term reduction in ecosystem flammability, driving a decline in charcoal influx despite climatic changes (Blyakharchuk et al., 2013; Blyakharchuk, 2020).

In Region G, a disconnect emerges in the late Holocene: despite a humid climate that should support biomass, charcoal influx declined (Unkelbach et al., 2021; Barhoumi et al., 2024). This anomaly is attributed to anthropogenic landscape fragmentation caused by intense grazing (Zhang et al., 2021). As observed in modern studies, livestock remove fine surface fuels, effectively severing fuel connectivity and suppressing fire spread (Umbanhowar et al., 2009).

Broadly, Holocene fire regimes in the Altai-Sayan Mountains and adjacent plains reflect a shift from climate-limited systems to human-modified systems. Before  $\sim 2$  cal. kyr BP, fire activity was largely regulated by moisture (limiting fuel in steppe regions A & G) or temperature (limiting fuel in alpine/forest regions E & F). Since  $\sim 2$  cal. kyr BP, a divergence occurs: in regions with expanding agriculture/pastoralism (A, B, C, D), anthropogenic ignition sources amplified fire activity beyond natural baselines. Conversely, in heavily grazed areas (Region G), pastoral pressure fragmented fuels, suppressing fires. This synthesis highlights the fundamental transition of the Altai-Sayan fire regime from biophysical control to anthropogenic dominance in the late Holocene.

## 5 Conclusions

This study presents a long-term fire record from western Mongolia and systematically evaluates the spatiotemporal variations in charcoal influx and its coupling with vegetation across the Altai-Sayan Mountains and adjacent plains. Our synthesis reveals distinct regional drivers of fire regimes rooted in climate-fuel feedbacks and, more recently, anthropogenic forcing:

Prior to  $\sim 2$  cal. kyr BP: Fire activity was primarily regulated by biophysical constraints on fuel availability. In the steppe zone (Region A), low charcoal influx was driven by aridity, which limited vegetation productivity and fuel continuity. In the Central Altai forests (Regions D and E) and Western Sayan (Region F), fire trends generally followed temperature-regulated forest dynamics. Specifically, the early-to-mid Holocene decline in charcoal influx (Regions D, E, and F) reflected shifts in forest composition and cover. Notably, in Region F, this decline was mechanistically linked to the expansion of fire-resistant *P. sylvestris*, which reduced ecosystem flammability by displacing more combustible taxa.

A synchronized surge since  $\sim 2$  cal. kyr BP in charcoal influx occurred across Regions A, B, C and D. This widespread intensification was driven by the synergistic effects of regional climatic changes and intensified human activities (e.g., agricultural expansion and pastoral burning), which overrode natural fuel limitations. Conversely, Region G exhibited a marked decline in charcoal influx despite favorable climatic conditions. This anomaly is attributed to landscape fragmentation caused by intensive grazing, where livestock pressure reduced surface fuels and suppressed fire spread.

Our findings underscore that fire regimes in the Altai-Sayan ecoregion are determined not just by climate, but by the specific flammability traits of dominant vegetation (e.g., pyrophytic *Betula/Larix* vs. fire-resistant *P. sylvestris*) and land-use history. Understanding these long-term fire-vegetation-human interactions provides critical baselines for predicting future wildfire risks and implementing sustainable forest management strategies in a warming world.

**Code availability.** This study did not develop any new software code; all analyses were conducted using standard publicly available software/packages as cited in the text.

**Data availability.** All data generated for this paper will be shared based on the reasonable request.

**Supplement.** The supplement related to this article is available online at <https://doi.org/10.5194/cp-22-445-2026-supplement>.

**Author contributions.** D.L. Z.: Writing – review & editing, Validation, Methodology, Funding acquisition, Conceptualization. B. T., A.Z. S., and X.Z. H.: Writing – original draft, Visualization, Methodology, Data curation. Y.J. L. – Data curation.

**Competing interests.** The contact author has declared that none of the authors has any competing interests.

**Disclaimer.** Publisher's note: Copernicus Publications remains neutral with regard to jurisdictional claims made in the text, published maps, institutional affiliations, or any other geographical representation in this paper. The authors bear the ultimate responsibility for providing appropriate place names. Views expressed in the text are those of the authors and do not necessarily reflect the views of the publisher.

**Acknowledgements.** We thank anonymous reviewers and editor for their valuable comments, which significantly improved the manuscript.

**Financial support.** This research has been supported by the National Natural Science Foundation of China (grant no. 42471183), Youth Innovation Promotion Association of Chinese Academy of Sciences (grant no. 2022447), National Natural Science Grants of China (grant no. 42220104001) and Russian Budget project (grant no. FWRG-2026-0007).

**Review statement.** This paper was edited by Natalia Piotrowska and reviewed by two anonymous referees.

## References

- Agatova, A. R., Nepop, R. K., Bronnikova, M. A., Slyusarenko, I. Y., and Orlova, L. A.: Human occupation of South Eastern Altai highlands (Russia) in the context of environmental changes, *Archaeol. Anthropol. Sci.*, 8, 419–440, <https://doi.org/10.1007/s12520-014-0202-7>, 2016.
- Aizen, E. M., Aizen, V. B., Melack, J. M., Nakamura, T., and Ohta, T.: Precipitation and atmospheric circulation patterns at mid-latitudes of Asia, *Int. J. Climatol.*, 21, 535–556, <https://doi.org/10.1002/joc.626>, 2001.
- Albrich, K., Rammer, W., Thom, D., and Seidl, R.: Trade-offs between temporal stability and level of forest ecosystem services provisioning under climate change, *Ecol. Appl.*, 28, 1884–1896, <https://doi.org/10.1002/eap.1785>, 2018.
- Barhoumi, C., Bliedtner, M., Zech, R., and Behling, H.: Holocene vegetation, fire, climate dynamics and human impact in the upper Orkhon Valley of the Khangai Mountains, Mongolia, *Quat. Sci. Rev.*, 334, 108713, <https://doi.org/10.1016/j.quascirev.2024.108713>, 2024.
- Blyakharchuk, T. A.: Dynamics of vegetation cover and quantitative palaeoclimatic reconstructions in the Western Sayan Mountains from the Late Glacial period to the present time according to

- a palynological study of the Yuzhno-Buybinskoe mire, in: IOP Conference Series: Earth and Environmental Science, 611, 1, 012026, <https://doi.org/10.1088/1755-1315/611/1/012026>, 2020.
- Blyakharchuk, T. A. and Chernova, N. A.: Vegetation and climate in the Western Sayan Mts according to pollen data from Lugovoe Mire as a background for prehistoric cultural change in southern Middle Siberia, *Quat. Sci. Rev.*, 75, 22–42, <https://doi.org/10.1016/j.quascirev.2013.05.017>, 2013.
- Blyakharchuk, T. A. and Pupysheva, M. A.: Indication of fires in the thousand-year history of Central Altai, *Geography and Natural Resource*, 4, 128–136, [https://doi.org/10.15372/GIPR20220415\\_2022](https://doi.org/10.15372/GIPR20220415_2022) (in Russian).
- Blyakharchuk, T. A., Wright, H. E., Borodavko, P. S., van der Knaap, W. O., and Ammann, B.: Late Glacial and Holocene vegetational changes on the Ulagan high-mountain plateau, Altai Mountains, southern Siberia, *Palaeogeogr. Palaeoclimat. Palaeoecol.*, 209, 259–279, <https://doi.org/10.1016/j.palaeo.2004.02.011>, 2004.
- Blyakharchuk, T. A., Wright, H. E., Borodavko, P. S., van der Knaap, W. O., and Ammann, B.: Late glacial and Holocene vegetational history of the Altai mountains (southwestern Tuva Republic, Siberia), *Palaeogeogr. Palaeoclimat. Palaeoecol.*, 245, 518–534, <https://doi.org/10.1016/j.palaeo.2006.09.010>, 2007.
- Blyakharchuk, T. A., Wright, H. E., Borodavko, P. S., van der Knaap, W. O., and Ammann, B.: The role of pingos in the development of the Dzhangyskol lake-pingo complex, central Altai Mountains, southern Siberia, *Palaeogeogr. Palaeoclimat. Palaeoecol.*, 257, 404–420, <https://doi.org/10.1016/j.palaeo.2007.09.015>, 2008.
- Blyakharchuk, T. A., van Hardenbroek, M., Pupysheva, M. A., Kirpotin, S. N., and Blyakharchuk, P. A.: Late Glacial and Holocene history of climate, vegetation landscapes and fires in South Taiga of Western Siberia based on radiocarbon dating and multi-proxy palaeoecological research of sediments from Shchuchye Lake, *Radiocarbon*, 1–24, <https://doi.org/10.1017/RDC.2024.103>, 2024.
- Blaauw, M. and Christen, J. A.: Flexible paleoclimate age-depth models using an autoregressive gamma process, *Bayesian Analysis*, 6, 457–474, <https://doi.org/10.1214/11-BA618>, 2011.
- Chen, X.: *Geography of Chinese Arid Region*, Science Press, Beijing, ISBN 9787030275837, 2010 (in Chinese).
- Feng, Z. D., Sun, A. Z., Abdusalih, N., Ran, M., Kurban, A., Lan, B., Zhang, D. L., and Yang, Y.: Vegetation changes and associated climatic changes in the southern Altai Mountains within China during the Holocene, *Holocene*, 27, 683–693, <https://doi.org/10.1177/0959683616670469>, 2017.
- Feurdean, A., Florescu, G., Tanțău, I., Vanni ere, B., Diaconu, A. C., Pfeiffer, M., and Kirpotin, S.: Recent fire regime in the southern boreal forests of western Siberia is unprecedented in the last five millennia, *Quat. Sci. Rev.* 244, 106495, <https://doi.org/10.1016/j.quascirev.2020.106495>, 2020.
- Feurdean, A., Diaconu, A.-C., Pfeiffer, M., Gaika, M., Hutchinson, S. M., Butiseaca, G., Gorina, N., Tonkov, S., Niamir, A., Tantau, I., Zhang, H., and Kirpotin, S.: Holocene wildfire regimes in western Siberia: interaction between peatland moisture conditions and the composition of plant functional types, *Clim. Past*, 18, 1255–1274, <https://doi.org/10.5194/cp-18-1255-2022>, 2022.
- Fu, B. J., Liu, G. H., and Ouyang, Z. Y.: *Ecological regionalization in China*, Beijing, Science Press, ISBN 9787030381682, 2013 (in Chinese).
- Furyaev, V. V.: *Role of Fire in Forest Development*, Nauka Publications, Novosibirsk, 1996 (in Russian).
- Goldammer, J. G. and Furyaev, V.: *Fire in ecosystems of boreal Eurasia*, Vol. 48, Springer Science & Business Media, <https://doi.org/10.1007/978-94-015-8737-2>, 2013.
- Hu, Y., Huang, X., Demberel, O., Zhang, J., Xiang, L., Gundegmaa, V., and Chen, F.: Quantitative reconstruction of precipitation changes in the Mongolian Altai Mountains since 13.7 ka, *Catena*, 234, 107536, <https://doi.org/10.1016/j.catena.2023.107536>, 2024.
- Hu, Y., Huang, X., Li, Y., Chen, H., Demberel, O., Zhang, J., and Xiao, J.: Holocene fire dynamics in the Altai Mountains and its driving factors, *Geophys. Res. Lett.*, 52, e2025GL116309, <https://doi.org/10.1029/2025GL116309>, 2025.
- Ivanova, G. A., Kukavskaya, E. A., Ivanov, V. A., Conard, S. G., and McRae, D. J.: Fuel characteristics, loads and consumption in Scots pine forests of central Siberia, *J. Forestry Res.*, 31, 2507–2524, <https://doi.org/10.1007/s11676-019-01038-0>, 2020.
- Jones, M. W., Smith, A., Betts, R., Canadell, J. G., Prentice, I. C., and Le Qu er e, C.: Climate change increases the risk of wildfires, *ScienceBrief Rev.*, 116, 117, <https://www.jstor.org/stable/resrep51248>, 2020.
- Kasischke, E. S.: Boreal ecosystems in the global carbon cycle, in: *Fire, Climate Change, and Carbon Cycling in the Boreal Forest*, edited by: Kasischke, E. S. and Stocks, B. J., Ecological, <https://doi.org/10.1007/978-0-387-21629-4>, 2000.
- Kharuk, V. I., Ponomarev, E. I., Ivanova, G. A., Dvinskaya, M. L., Coogan, S. C., and Flannigan, M. D.: Wildfires in the Siberian taiga, *Ambio*, 50, 1953–1974, <https://doi.org/10.1007/s13280-020-01490-x>, 2021.
- Kutzbach, J. E., Chen, G., Cheng, H., Edwards, R. L., and Liu, Z.: Potential role of winter rainfall in explaining increased moisture in the Mediterranean and Middle East during periods of maximum orbitally-forced insolation seasonality, *Clim. Dyn.*, 42, 1079–1095, <https://doi.org/10.1007/s00382-013-1692-1>, 2014.
- L ezine, A. M., Izumi, K., and Achoundong, G.: Mbi Crater (Cameroon) illustrates the relations between mountain and lowland forests over the past 15,000 years in western equatorial Africa, *Quat. Int.*, 657, 67–76, <https://doi.org/10.1016/j.quaint.2020.12.014>, 2023.
- Li, Y., Zhang, Y., Wang, J., Wang, L., Li, Y., Chen, L., Zhao, L., and Kong, Z.: Preliminary study on pollen, charcoal records and environmental evolution of Alahake Saline Lake in Xinjiang since 4,700 cal yr BP, *Quat. Int.*, 513, 8–17, <https://doi.org/10.1016/j.quaint.2019.01.014>, 2019.
- Li, Y., Zhang, D., Zhang, Y., Sun, A., Li, X., Huang, X., Zhang, Y., and Li, Y.: Distentangling the late-Holocene human–environment interactions in the Altai Mountains within the Arid Central Asia, *Palaeogeogr. Palaeoclimat. Palaeoecol.*, 654, 112466, <https://doi.org/10.1016/j.palaeo.2024.112466>, 2024.
- Liu, F., Liu, H., Xu, C., Shi, L., Zhu, X., Qi, Y., and He, W.: Old-growth forests show low canopy resilience to droughts at the southern edge of the taiga, *Global Change Biol.*, 27, 2392–2402, <https://doi.org/10.1111/gcb.15605>, 2021.
- Marcott, S. A., Shakun, J. D., Clark, P. U., and Mix, A. C.: A reconstruction of regional and global tempera-

- ture for the past 11,300 years, *Science*, 339, 1198–1201, <https://doi.org/10.1126/science.1228026>, 2013.
- Mo, L., Zohner, C. M., Reich, P. B., Liang, J., De Miguel, S., Nabuurs, G. J., and Ortiz-Malavasi, E.: Integrated global assessment of the natural forest carbon potential, *Nature*, 624, 92–101, <https://doi.org/10.1038/s41586-023-06723-z>, 2023.
- Panyushkina, I. P.: Climate-Induced changes in Population Dynamics of Siberian Scythians (700–250 B.C.). *Climate, Landscapes and Civilizations*, Geogra. Monograph Series, 198, 145–154, <https://doi.org/10.1029/GM198>, 2012.
- Ponomarev, E. I. and Kharuk, V. I.: Wildfire occurrence in forests of the Altai-Sayan region under current climate changes, *Contemp. Probl. Ecol.*, 9, 29–36, <https://doi.org/10.1134/S199542551601011X>, 2016.
- Power, M. J., Marlon, J., Ortiz, N., Bartlein, P. J., Harrison, S. P., Mayle, F. E., and Zhang, J. H.: Changes in fire regimes since the Last Glacial Maximum: an assessment based on a global synthesis and analysis of charcoal data, *Clim. Dynam.*, 30, 887–907, <https://doi.org/10.1007/s00382-007-0334-x>, 2007.
- Reimer, P. J., Austin, W. E., Bard, E., Bayliss, A., Blackwell, P. G., Ramsey, C. B., and Talamo, S.: The IntCal20 Northern Hemisphere radiocarbon age calibration curve (0–55 cal kBP), *Radiocarbon*, 62, 725–757, <https://doi.org/10.1017/RDC.2020.41>, 2020.
- Rudaya, N., Sergey, K., Michał, S., Xianyong, C., and Snezhana, Z.: Postglacial history of the steppe Altai: climate, fire and plant diversity, *Quat. Sci. Rev.*, 249, 106616, <https://doi.org/10.1016/j.quascirev.2020.106616>, 2020.
- Rudoy, A. N. and Yatsuk, T. Y.: The palaeogeography of south-eastern Altai. *Chetvertichnaya geologiya i pervobytnaya arkheologiya*, Thesis of conference, Ulan-Ude, 73–75, 1986.
- Shi, C. M., Liang, Y., Gao, C., Wang, Q. H., and Shu, L. F.: Drought-modulated boreal forest fire occurrence and linkage with La Nina events in Altai Mountains Northwest China, *Atmosphere*, 11, 956, <https://doi.org/10.3390/atmos11090956>, 2020.
- Sun, A., Feng, Z. D., Ran, M., and Zhang, C. J.: Pollen-recorded bioclimatic variations of the last ~ 22,600 years retrieved from Aчит Nuur core in the western Mongolian Plateau, *Quat. Int.* 311, 36–43, <https://doi.org/10.1016/j.quaint.2013.07.002>, 2013.
- Slavnin, V. D. and Sherstova L. I.: *Aerchaologic-Ethnographic Essay of Northern Khakassia in the Area of Geological Polygon of Siberian High School*, Tomsk Polytechnical University Press, Tomsk, 1999 (in Russian).
- Tang, G., Yang, S., Miao, Y., Luo, Y.L., Chen, Z. X., and Liu, L.: Grain size characteristics of microfossil charcoal and the environmental implications in loess deposits from Ganzhi, Western Sichuan Plateau, *J. Lanzhou University (Natural Sci.)*, 58, 298–305, <https://doi.org/10.13885/j.issn.0455-2059.2022.03.003>, 2022 (in Chinese).
- Umbanhowar Jr., C. E., Shinneman, A. L., Tserenkhand, G., Hammon, E. R., Lor, P., and Nail, K.: Regional fire history based on charcoal analysis of sediments from nine lakes in western Mongolia, *Holocene*, 19, 611–624, <https://doi.org/10.1177/0959683609104039>, 2009.
- Unkelbach, J., Dulamsuren, C., Klinge, M., and Behling, H.: Holocene high-resolution forest-steppe and environmental dynamics in the Tarvagatai Mountains, northcentral Mongolia, over the last 9570 cal yr BP, *Quat. Sci. Rev.*, 266, 107076, <https://doi.org/10.1016/j.quascirev.2021.107076>, 2021.
- Wang, W., Ma, Y. Z., Feng, Z. D., Narantsetseg, Ts, Liu, K. B., and Zhai, X. W.: A prolonged dry mid-Holocene climate revealed by pollen and diatom records from Lake Uggii Nuur in central Mongolia, *Quat. Int.*, 229, 74–83, <https://doi.org/10.1016/j.quaint.2010.06.005>, 2011.
- Wang, Z., Miao, Y., Zhao, Y., Zhang, Z., Zou, Y., and Zhang, T.: Preliminary exploration of the fire activity recorded by microcharcoal in surface sediments of Central and Western China, *Quat. Sci.*, 44, 201–213, <https://doi.org/10.11928/j.issn.1001-7410.2024.01.15>, 2024 (in Chinese).
- Wood, S. N.: *Generalized Additive Models: An Introduction with R (2nd Edition)*, Chapman and Hall/CRC, 1–476, <https://doi.org/10.1201/9781315370279>, 2017.
- Xiao, Y., Xiang, L., Huang, X., Mills, K., Zhang, J., Chen, X., and Li, Y.: Moisture changes in the northern Xinjiang basin over the past 2400 years as documented in pollen records of Jili Lake, *Front. Earth Sci.*, 9, 741992, <https://doi.org/10.3389/feart.2021.741992>, 2021.
- Xiang, L., Huang, X., Sun, M., Panizzo, V. N., Huang, C., Zheng, M., and Chen, F.: Prehistoric population expansion in Central Asia promoted by the Altai Holocene climatic optimum, *Nat. Commun.*, 14, 3102, <https://doi.org/10.1038/s41467-023-38828-4>, 2023.
- Xinjiang Comprehensive Expedition Team, Institute of Botany, Chinese Academy of Sciences: *Vegetation and its utilization in Xinjiang*, Beijing, Science Press, 1978.
- Zhang, D. L. and Feng, Z. D.: Holocene climate variations in the Altai Mountains and the surrounding areas: a synthesis of pollen records, *Earth Sci. Rev.*, 185, 847–869, <https://doi.org/10.1016/j.earscirev.2018.08.007>, 2018.
- Zhang, D., Chen, X., Li, Y., Wang, W., Sun, A., Yang, Y., and Feng, Z.: Response of vegetation to Holocene evolution of westerlies in the Asian Central Arid Zone, *Quat. Sci. Rev.*, 229, 106138, <https://doi.org/10.1016/j.quascirev.2019.106138>, 2020.
- Zhang, D., Huang, X., Liu, Q., Chen, X., and Feng, Z.: Holocene fire records and their drivers in the westerlies-dominated Central Asia, *Sci. Total Environ.*, 833, 155153, <https://doi.org/10.1016/j.scitotenv.2022.155153>, 2022.
- Zhang, S. J., Lu, Y., Wei, W., Qiu, M., Dong, G., and Liu, X.: Human activities have altered fire-climate relations in arid Central Asia since ~ 1000 a BP: evidence from a 4200-year-old sedimentary archive, *Sci. Bull.*, 66, 761–764, <https://doi.org/10.1016/j.scib.2020.12.004>, 2021.
- Zhang, Y. Y. and Zhang, D. L.: Spatiotemporal patterns of pollen-based Holocene precipitation variations in the Altai Mountains and the surrounding areas, *Global Planet. Change*, 251, 104832, <https://doi.org/10.1016/j.gloplacha.2025.104832>, 2025.
- Zheng, B., Ciais, P., Chevallier, F., Yang, H., Canadell, J. G., Chen, Y., and Zhang, Q.: Record-high CO<sub>2</sub> emissions from boreal fires in 2021, *Science*, 379, 912–917, <https://doi.org/10.1126/science.ade0805>, 2023.